10th International Symposium on the Science and Processing of Cast Iron – SPCI10

Analytical Functions Describing Solidification of Gray Cast Iron based on Thermodynamic Calculations

S. Jonsson*
Department of Materials Science and Engineering, Royal Institute of Technology,
SE-100 44, Stockholm, Sweden

Thermodynamic calculations and Scheil-Gulliver simulations are used for simulating solidification of gray cast iron, systematically varying the composition around Fe-3.35C-2Si by adding Cr, Ni, Mn, Mo, Cu, S, P, and in some cases, Al, V, and B. By adding Ti and N, the competition between Ti(C,N) and N_2-gas precipitation is thoroughly studied.
The simulated results are assessed by regression analysis producing many explicit formulae for predicting solidification of gray cast iron. The agreement between thermodynamic calculations and regression formulae is generally very good.

Keywords: gray cast iron, solidification simulations, Scheil-Gulliver simulations, liquidus projections, analytical functions.

Introduction

As process control of casting becomes more important, the interest in solidification simulations increases as they offer a way of predicting and understanding effects from variations in chemical composition. However, in order to be successful with simulations, proper thermodynamic software, high-quality databases and computational skills are needed. This is difficult for industry to meet and besides, time consuming simulations are not appealing when quick decisions are to be taken. An alternative is to make lots of simulations in advance, systematically varying the composition and modeling the results of important quantities with explicit analytical functions. These functions can then be used to quickly predict the casting behavior of an alloy, assisting industrial process control. They can also be used in more advanced simulations where the variations of solidification parameters with composition are needed. This is exactly was has been done in the present work, obtaining a remarkably high precision of the analytical descriptions.

Calculating Procedure

All calculations were performed using Thermo-Calc[1,2] and its TCFE4 databank. The thermodynamic information has previously been assessed by the CALPHAD method[3,4] and is not compared to any experimental results in the present work. The total size of the calculated system was fixed to 1 mole of atoms applying a total pressure of 1 bar, unless stated otherwise. All compositions are given in weight percent, as normally done in industry.

In general, two computational techniques can be used for solidification, equilibrium calculations and Scheil-Gulliver simulations[5-7], respectively. The former predicts the equilibrium state which, in practice, may need considerable time to be reached. The latter is a simulation with many equilibrium calculations at continuously decreasing temperature, starting in the melt and ending at a preset fraction of remaining liquid, as 3%, for instance. During simulations using the Scheil-Gulliver module of the Thermo-Calc software, the composition of the liquid phase follows the liquidus surface and can easily be tracked in calculated diagrams. However, as the solid phases receives different composition during formation their average composition must be integrated. The option of using fast-diffusing elements was tested for C and N, but resulted in small differences compared to slow diffusion, why it was not used in the present work. The Scheil-Gulliver simulation technique has been described in more detailed by Kozeschnik[8], for instance.

The calculations started in the Fe-C diagram adding Si. Then, a base alloy of Fe-C-2Si was used adding another element, and so on. In general, no cross-correlation effects among the added elements were explored, unless they formed precipitates. Each element was added with incremental amounts, to levels far above compositions normally found in gray cast irons. The extended composition range allows extrapolations to be safer. For each quantity to be modeled, the base functions were carefully selected to be able to reproduce the result as accurately as possible.

Fe-C-Si

The effect of Si on the Fe-C system is seen in Fig. 1. In a) it is seen that the eutectic point and the liquidus surfaces are pushed towards Fe. This is consistent with b) showing the liquidus projection. Here the liquidus fcc/graph trough demonstrates the displacement of the eutectic point (towards Fe) with Si-additions. Naturally, the carbon equivalent, C_{eq}, is parallel to this line. As seen, the isotherms are also parallel to the fcc/graph liquidus trough implying that they are

* Email: jonsson@kth.se

closely related to C_{eq}. This is demonstrated in Fig. 2a showing the liquidus temperature for Fe-C-2Si with carbon content between 3.20 and 3.55wt%. The carbon content is here calculated from a regression analysis.

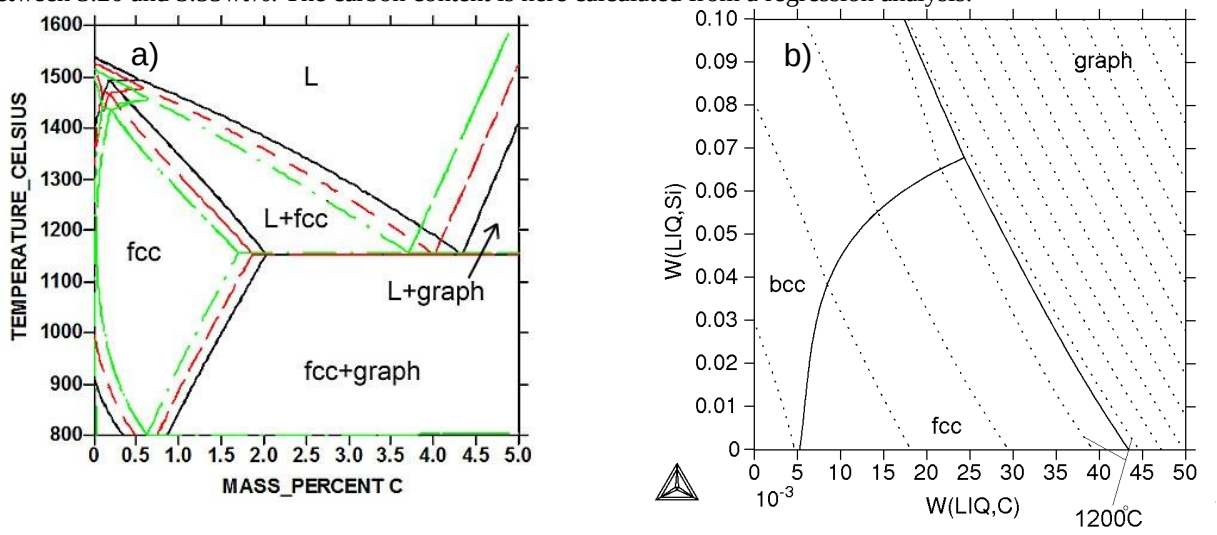

Fig.1: a) Fe-C diagram with additions of 1 (red, dashed) and 2wt% (green, dash-dotted) of Si.
b) Liquidus projection of Fe-C-Si (in weight fractions) with dotted liquidus isotherms in 100°C intervals.

As solidification of hypoeutectic alloys starts with proeutectic precipitation of fcc, the composition of the melt moves away from Fe, along an almost straight line (close to horizontal, slightly pointing down in Fig. 1b, until it reaches the fcc/graph trough. As a result of the straight path, the amount of proeutectic fcc is also closely related to the carbon equivalent. This is demonstrated in Fig. 2b.

Another factor controlling the amount of proeuctectic fcc is the undercooling. The effect can easily be simulated by rejecting graphite in the simulations. Then, the solidification path continues beyond the fcc/graph trough and the additional fraction because of undercooling can be obtained. It could be perfectly described by a second degree polynomial.

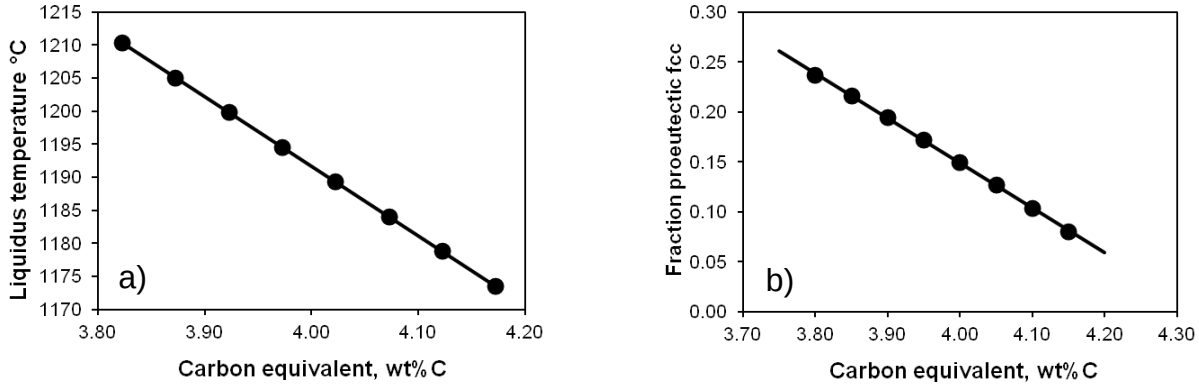

Fig.2: a) Liquidus temperature and b) fraction of proeutectic fcc, as function of C_{eq}.

Fe-C-2Si-X

As Si is always added to gray cast iron, the calculations continued with exploring the effects of adding a fourth element, X, to the Fe-C-2Si, system. Two such calculations are shown in Fig. 3. Here the x-axis is identical to a line drawn in Fig. 1b at 2% Si. As seen in Fig. 3, Cr pushes the fcc/graph trough towards higher C-content, whereas Cu pushes it towards lower. As before, the liquidus isotherms follow the trough. In Fig. 3a, cementite and M_7C_3 carbides are predicted to precipitate from the liquid at high Cr-content. In Fig. 3b, a miscibility gap, L#2, is predicted. These findings come from the TCFE4 databank and it could be emphasized that no attempts were made to find out if these predictions are relevant or not. The present work is a direct result of the information in the thermodynamic databank.

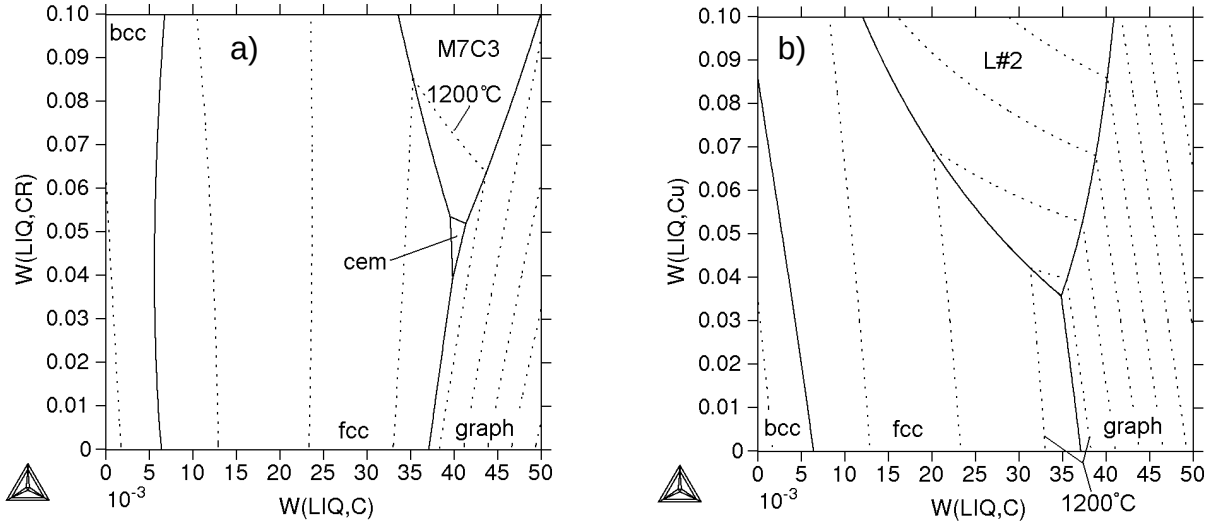

Fig.3: Liquidus projection with dotted liquidus isotherms for Fe-C-2Si adding a) Cr and b) Cu.

The combined result from adding various elements is seen in Fig. 4a. As seen, quite straight lines are obtained which is a consequence of the fcc/graph trough being almost straight, as clearly demonstrated in Fig. 3. Naturally, the added elements will also influence the amount of proeutectic fcc. The effects from various elements are demonstrated for an Fe-3.35C-2Si alloy in Fig. 4b.

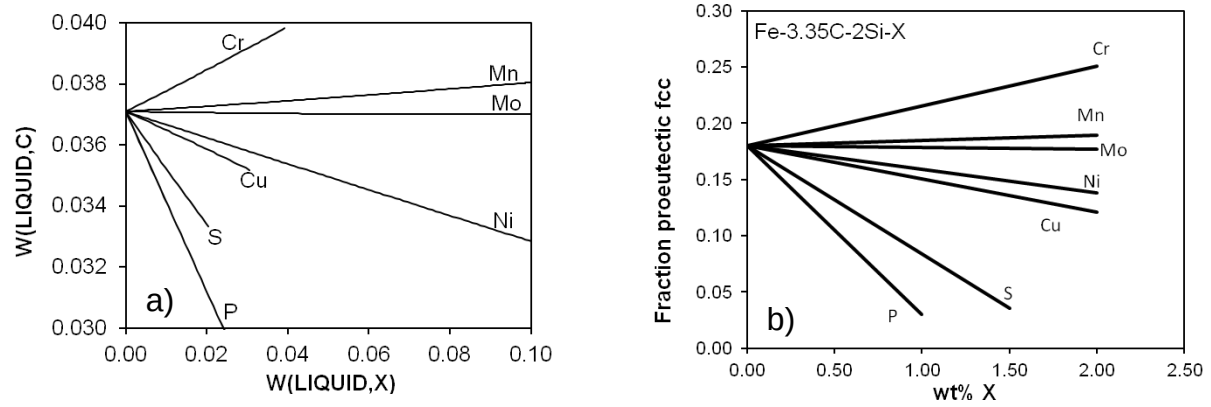

Fig.4: Influence of X-addition on a) the eutectic carbon content and b) fraction proeutectic fcc in Fe-3.35C-2Si.

Finally, the influence on the eutectic temperature was calculated for the Fe-C-2Si system with additions of X. The result is shown in Fig. 5.

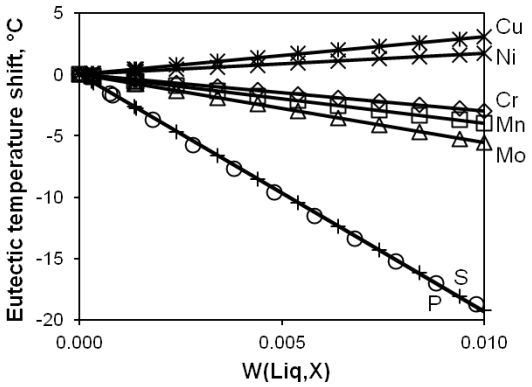

Fig.5: Influence on the eutectic temperature by X-additions to Fe-C-2Si.

Precipitations

Calculations for the Fe-C-2Si system showed that the lowest Ti or Nb content, needed for precipitation of TiC or NbC from the melt, is found at the eutectic point. For Ti the lowest value is 0.148 and for Nb it is 0.059 wt%. Both values are considerably higher than industrial maximum levels. Hence, precipitation of TiC or NbC from the melt was not considered further. Instead, N was added to the system allowing precipitation of Ti(C,N) but also of N_2-gas, G. By performing calculations for the alloy, Fe-3.7C-2Si-0.015N-0.025Ti-0.003B-0.003Al-0.01V-0.02Nb, considered having maximum industrial levels of precipitation forming elements, it was concluded that the only additional precipitate from the melt was AlN.

In order to explore precipitation of Ti(C,N), a series of calculations with different amounts of Ti was performed in the Fe-C-2Si-Ti-N system under 1 bar of pressure. The results are shown in Fig. 6. As seen, a large field for G is found in the upper part of the diagrams. As the Ti-level is increased, an area for Ti(C,N) forms in the triple point of the fcc+graph+G phases and extends over these phases. It is interesting to note that only a minute amount of N is needed to form Ti(C,N) close to the fcc/graph eutectic even for low amounts of Ti. As stated above, the Ti(C,N) field is not reaching the x-axis until 0.148% Ti is added. In practice when nitrogen is present, a wide Ti(C,N)-field is formed for much lower Ti-levels.

As demonstrated by the calculations, the Ti(C,N) field is formed between fcc and G. In this respect it protects the melt from formation of gas bubbles as the upper level for N_2-precipitation is set by the Ti(C,N)/G phase boundary. Scheil-Gulliver simulations for Fe-3.33C-2Si-0.010N alloys with 0 and 0.015%Ti are shown as red broken lines in Fig. 6a and d, respectively. (Here 3.33%C was used rather than 3.35% in order to displace the C-content a bit away from the triple point rendering clearer figures.) The same simulations are shown in Fig. 7a, but now demonstrating the precipitated amount in mole of N_2-gas, NP(G), as function of temperature. Both solidifications start with precipitation of gas. Without Ti, precipitation continues until the fcc/G boundary is reached, but with 0.015%Ti, it stops practically when the Ti(C,N)/G boundary is reached. By extrapolating the fcc/graph, fcc/G and graph/G boundaries into the Ti(C,N) phase field, Fig. 6d, it can clearly be seen that the solidification path follows the extrapolated boundaries. A similar situation is found when Ti is substituted by Al, Fig. 7b.

It should be noted that the values on the y-axes in Fig. 6 and 7b are 100 times smaller than on the x-axes. As a consequence, the small compositional changes on the y-axes during precipitation of Ti(C,N) cannot result in any noticeable change on the x-axes. Thus, the solidification paths are vertical until fcc starts to precipitate. Naturally, neither G nor AlN can alter the carbon content of the melt during their precipitation, as C is not a constituent in these phases.

It is evident that precipitation of Ti(C,N) or AlN limits the formation of gas bubbles. However, from Fig. 7a, it may be suggested that the casting temperature will not be high enough for any gas precipitation during casting. Already 0.015% Ti raises the onset temperature of gas precipitation from around 1200 to around 1340°C. (See the upper temperatures of the red lines in Fig. 7a.) Thus, if Ti(C,N) or AlN are precipitated from the liquid before casting starts, formation of gas bubbles should be strongly suppressed. Naturally, there is a competition between N_2-gas formation and Ti(C,N) precipitation as temperature is decreased. The outcome is determined by the thermodynamics and the starting compositions.

Analytical functions

The analytical functions, obtained from regression analyses of numerous simulations, are collected in the appendix. Many of them are polynomials with different powers of the alloying elements, which are always given in wt%. Some of them are a bit more complicated and will be commented on closer.

Equations 1-3 give values of the carbon content in wt%. The first two are well known, the eutectic carbon content, C_{eut}, and the carbon equivalent, C_{eq}, respectively. The third one, C_{Tliq}, is the carbon content needed for being on the L/L+fcc liquidus surface at a temperature given by T_{liq} in °C.

Equations 4 and 5 give temperatures in °C of the L/L+fcc liquidus temperature, T_{liq} and the eutectic temperature, T_{eut}, respectively. Equation 6 gives the fraction of proeutectic fcc, f_{profcc}, forming between the temperatures of eq. 4 and 5. An undercooling ΔT, counted as positive, is included in order to account for delayed nucleation of graphite.

In the Fe-C-2Si-Ti-N system, the solubility product of Ti(C,N) in equilibrium with graphite can be modeled using the product of the weight fractions of Ti and N, w_{Ti} and w_N, as the carbon content can be approximated as constant. Equation 7a gives the solubility product and 7b the precipitation temperature (T in °C) of Ti(C,N) in equilibrium with graphite. The formulae uses the activity of nitrogen, a_N, which is related to the partial pressure of nitrogen through eq. 8.

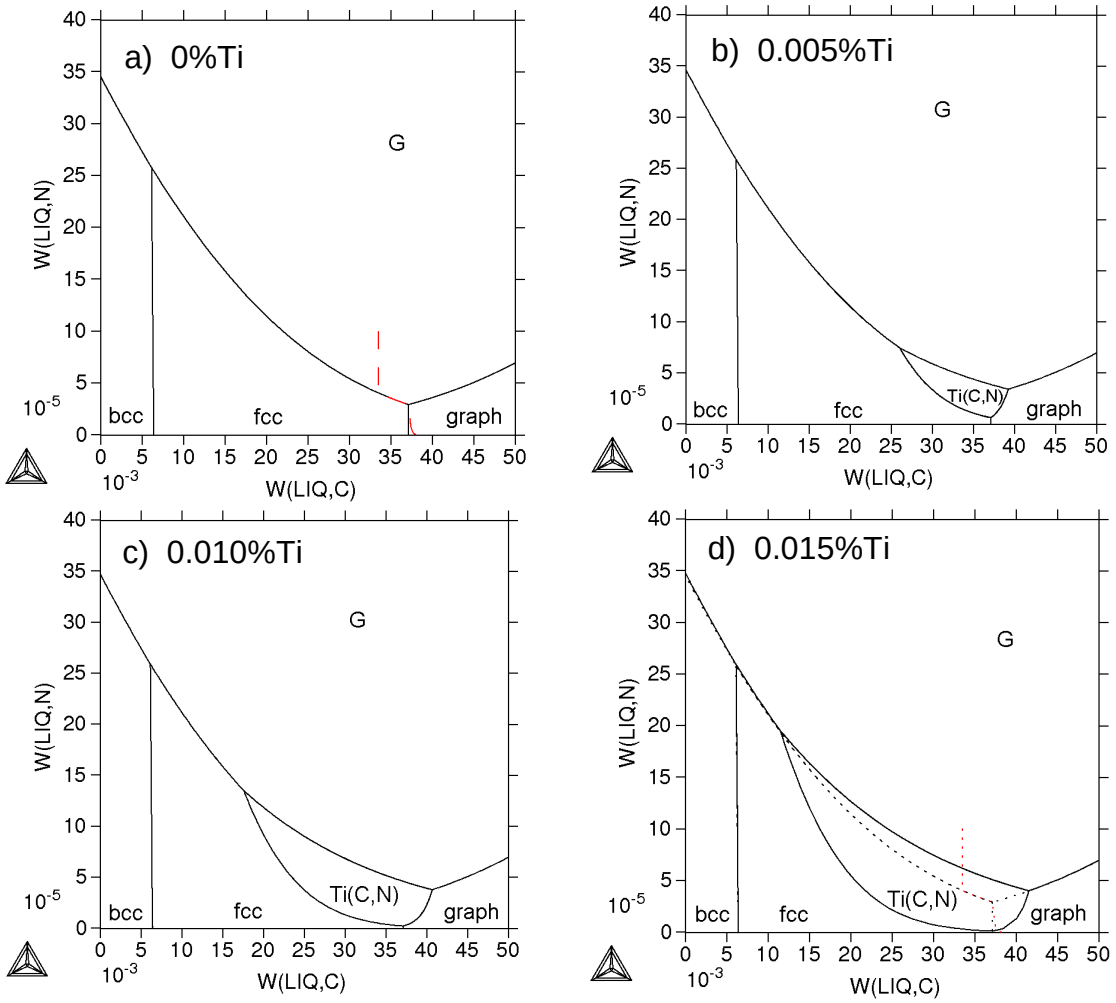

Fig.6: Influence on the liquidus projection by Ti-additions to Fe-C-2Si-N. Red lines show Scheil-Gulliver simulations for alloy compositions indicated in the text. Black dotted lines in d) are extrapolations of fcc/graph, fcc/G and graph/G into the Ti(C,N) phase field

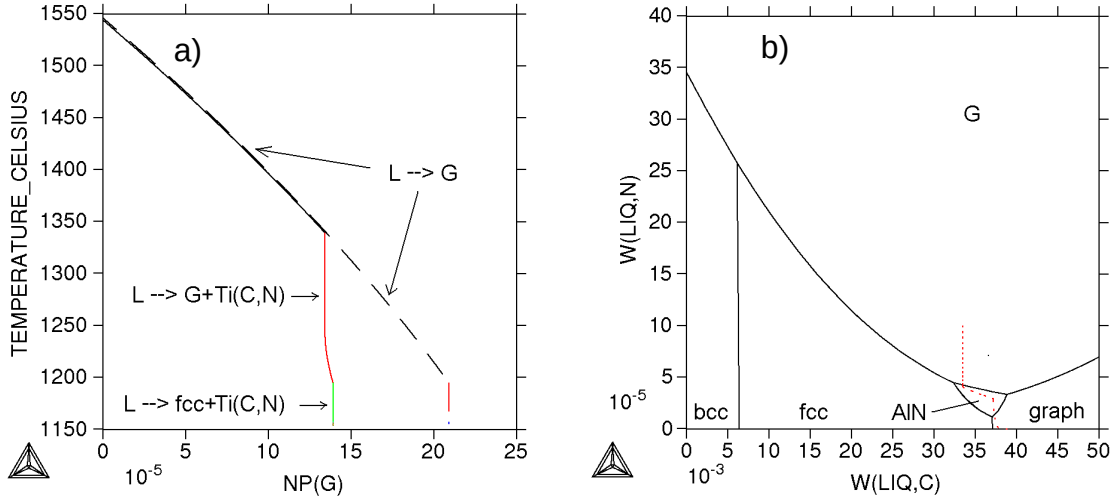

Fig.7: a) Scheil-Gulliver simulations of Fe-3.33C-2Si-0.010N with 0%Ti (dashed lines) and 0.015% Ti (solid line), showing precipitation of gas. b) Liquidus projection of Fe-C-2Si-0.004Al-N with Scheil-Gulliver simulation, (red dotted line).

The nitrogen content in the liquid at the onset of the eutectic solidification was evaluated for two conditions, one in equilibrium with N_2-gas at 1 bar without precipitation of Ti(C,N), eq. 9, N_{liq}(eut, G), the other in equilibrium with

Ti(C,N) without gas, eq. 10a and 10b, N_{liq}(eut, Ti(C,N)). The results were obtained from calculating the N-content in the liquid with varying Si content in the Fe-C-Si-N system. Then, additional calculations were performed in the Fe-C-2Si-N-X system. Naturally, the value of the α-parameter in 10b should be inserted into 10a. All compositions, including N, are given in wt%.

As seen from Fig. 6a, at 1 bar, the N-content of the fcc+G liquidus trough is carbon dependent. Naturally, it is also pressure dependent. By a series of calculations for the Fe-C-2Si-N system, the N-content of the fcc+G liquidus trough, N(fcc+G), could be evaluated, eq. 11. A similar analysis can be made for the Ti(C,N)+G liquidus appearing after Ti-additions, see Fig. 6b-d. Thus, the N-content of the Ti(C,N)+G liquidus trough was evaluated giving eq. 12 being similar to, but more complicated than eq 11. Another complication comes from the varying length of the Ti(C,N)+G boundary. The carbonitride is only precipitated within a carbon interval. This interval was evaluated and is given by eq. 13a. Thus, if eq 13a is not fulfilled, eq 12 cannot be used as no Ti(C,N) is formed. This condition is necessary, but not enough for Ti(C,N) to form. As seen from Fig. 6d, N(fcc+G) < N(Ti(C,N)+G) whenever Ti(C,N) is formed. Thus, this condition, eq. 13b, must also be obeyed if Ti(C,N) is precipitated instead of G.

As a melt cools, the nitrogen solubility reduces leading to gas precipitation. Scheil-Gulliver simulations showed that an Fe-3.35C-2Si-0.010N melt looses 0.035 mol N_2-gas per wt% evaporated N. Thus, the total amount of precipitated gas is this value multiplied by the difference between the original N-content, N, and the N-content at the onset of Ti(C,N) or fcc precipitation. This brings eq. 14 where the result from eq. 11 *or* 12 should be inserted, depending on the result of eqs. 13a and 13b. The result, NP(gas), is the number of moles of N_2-gas. By using the gas law and approximating the molar volume as M_{Fe}/ρ_{Fe} (molar weight and density of Fe) the volume fraction of gas can be found from eq. 15. Here R is the gas constant, 0.0821 $dm^3 \cdot atm \cdot K^{-1} \cdot mol^{-1}$ and p the nitrogen pressure in atm. For the simulations in the present work the amount of liquid, NP(liq), was set to 1 mol. By doing so, one finds that even small amounts of precipitated N, leads to large volumes of gas.

Scheil-Gulliver simulations in the Fe-3.35C-2Si-0.010N system with different amounts of Ti were used to evaluate the amount of precipitated Ti(C,N) when fcc starts to precipitate and when the eutectic solidification starts, respectively. The results were used to derive eqs. 16 and 17. Here f_{mass}(Ti(C,N),fcc) and f_{mass}(Ti(C,N),eutectic) refer to the mass fraction of Ti(C,N) for the respective reactions.

Accuracy

The accuracy of the analytical functions was tested against 5 test alloys, defined in Table 1. The first three test alloys represent a normal alloy, a low-alloyed and a highly alloyed alloy, with respect to nominal composition. The last two alloys are supposed to give minimum or maximum values of most of the tested quantities. The accuracy of the analytical functions is demonstrated in Fig. 8 for some quantities. In general, this good agreement was obtained between Thermo-Calc calculations and computed results from the regression formulae.

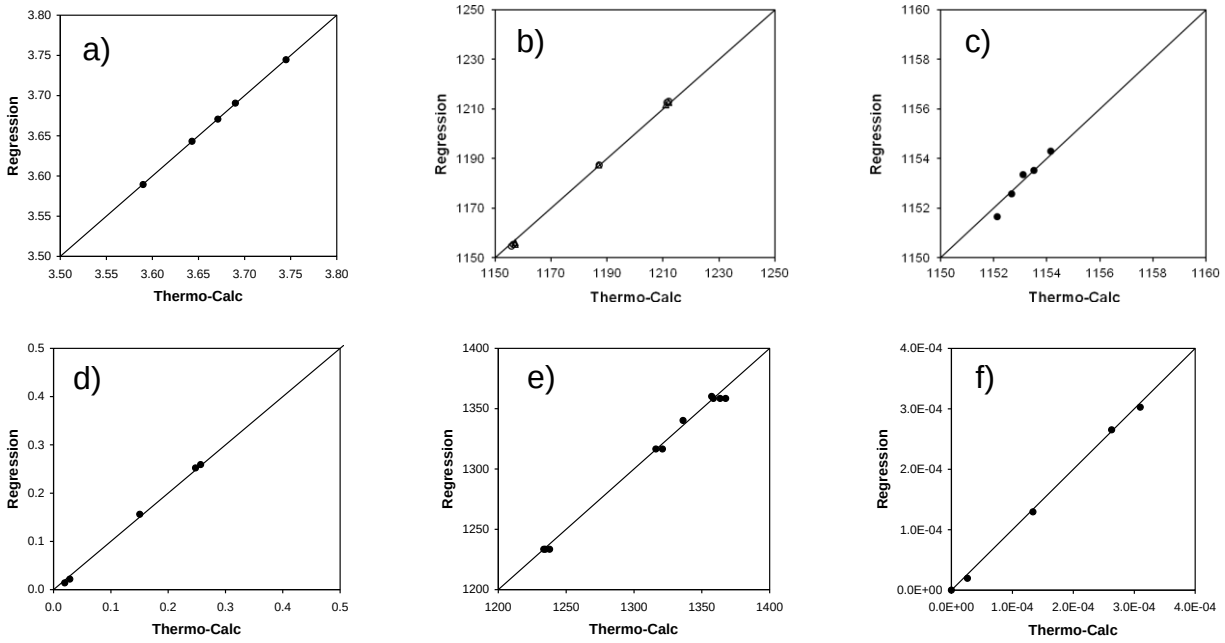

Fig.8: a) Eutectic carbon content (wt%C), b) Liquidus temperature (°C), c) Eutectic temperature (°C), d) Fraction proeutectic fcc, e) Precipitation temperature for Ti(C,N) in equilibrium with graphite (°C), f) Amount of precipitated N_2 during solidification (moles). Solid lines are guides to the eye, only.

Table 1: Composition, in wt%, of test alloys

Alloys	C	Si	P	S	Mn	Cr	Cu	Mo	Ni	N
Normal	3.35	2	0.03	0.07	0.6	0.3	0.6	0.05	0.02	0.010
Low all	3.2	1.8	0.01	0.05	0.4	0.2	0.4	0	0	0.010
High all	3.55	2.2	0.07	0.1	0.8	0.4	0.8	0.2	0.05	0.010
Min	3.55	1.8	0.07	0.1	0.4	0.2	0.8	0.2	0.05	0.010
Max	3.2	2.2	0.01	0.05	0.8	0.4	0.4	0	0	0.010

Discussion

A thermodynamic database has the advantage of combining many types of thermodynamic information. If the assessment is carefully done using consistent and complete data it is possible to obtain a good description of equilibrium conditions. The Scheil-Gulliver model simulates solidification from a homogeneous melt taking precipitation into account. Retarded nucleation, may give deviations in practice, but cannot be treated using Thermo-Calc. Only experimental testing of the functions supplied in the present work can tell how accurate they are and what adjustments may be needed. Evidently they give good descriptions of predictions based on the TCFE4 databank.

Conclusions

1. A number of explicit analytical equations were derived describing solidification of gray cast iron with nominal compositions around Fe-3.35C-2Si with additions of many alloying elements.
2. The agreement between analytical formulae and thermodynamic simulations is generally very good.
3. TiC is stabilized by small amounts of N making Ti(C,N) precipitation from liquid possible.
4. The onset of precipitation of Ti(C,N) or AlN stops precipitation of N_2-gas.

References

1. B. Sundman, B. Jansson, J. O. Andersson: *Calphad*, 1985, 9, 153-190.
2. J. O. Andersson, T. Helander, L. Höglund, P.F. Shi, B. Sundman: *Calphad* , 2002, 26, 273-312.
3. L. Kaufman, H Bernstein: "Computer Calculations of Phase Diagrams", Academic, New York (1970). See also the CALPHAD journal, Pergamon Press.
4. H.L. Lukas, S.G. Fries, B. Sundman: "Computational Thermodynamics – The Calphad Method" (2007), Cambridge.
5. G.H. Gulliver, *J. Inst. Met.* 1913, 9, 120-157.
6. E. Scheil, *Z. Metallkd*. 1942, 34, 70-72.
7. H. Fredriksson, U. Åkerlind: "Materials Processing during Casting", p. 185 (2006), Wiley.
8. E. Kozeschnik: *Metall. Mater. Trans. A*, 2000, 31A, 1682-1684.

Acknowledgement

This work was initiated by SCANIA CV AB, Södertälje, Sweden, and financially supported by DMMS, Design and Management of Manufacturing Systems, KTH, Stockholm, Sweden.

Appendix, Analytical functions

C_{eut} = 4.327-0.325Si+0.00679Si^2+0.0696Cr+0.00952Mn-0.000929Mo-0.0425Ni-0.0626Cu-0.184S-0.290P (1)

C_{eq} = C+0.325Si-0.00679Si^2-0.0696Cr-0.00952Mn+0.000929Mo+0.0425Ni+0.0626Cu+0.184S+0.290P (2)

C_{Tliq} = 15.34-0.009518T_{liq}-0.31Si+0.0072Si^2+0.027Cr-0.025Ni-0.034Mn-0.039Cu-0.058Mo-0.35S-0.46P (3)

T_{liq} = 1609.9-105.1C-32.6Si+0.76Si^2+2.84Cr-2.63Ni-3.57Mn-4.1Cu-6.1Mo-36.8S-48.3P (4)

T_{eut} = 1149.9+3.61Si+3.10Cu+1.71Ni-2.96Cr-3.95Mn-5.56Mo-19.3(S+P) (5)

f_{profcc} = 1.937-0.449C-0.146Si+0.00305Si^2+0.0355Cr+0.0046Mn-0.0017Mo-0.0211Ni-0.0295Cu
-0.0963S-0.150P+0.00392ΔT-1.05·10^{-5}ΔT^2 (6)

$$\log[w_{Ti}w_N] = 1.032 + 0.9105a_N - 0.199a_N^2 - \frac{15040 + 1030a_N - 220a_N^2}{T + 273} \quad (7a)$$

$$T + 273 = \frac{10000}{(-0.767 + 0.0505a_N - 0.011a_N^2) * \log(w_{Ti}) + 3.71 - 0.251a_N + 0.05a_N^2} \quad (7b)$$

$$a_N = \sqrt{p_{N_2}} \quad (8)$$

N_{liq}(eut,G) = 3.25·10^{-3}-1.79·10^{-4}Si+8.60·10^{-6}Si^2+2.39·10^{-4}Cr+5.86·10^{-5}Mn+2.87·10^{-6}Mn^2+5.00·10^{-5}Cu
-1.36·10^{-5}S+1.72·10^{-5}S^2-1.24·10^{-5}Mo-3.45·10^{-5}Ni-1.39·10^{-4}P (9)

$$N_{Liq}(eut, Ti(C,N)) = \left[\frac{\left(-1.298\cdot10^{-4} - 0.115Ti + 0.466Ti^2\right)\cdot\alpha + 8.6\cdot10^{-4} + 0.6256Ti - 3.874Ti^2}{Ti}\right]^{5.56} \quad (10a)$$

α = C-0.8080+0.4354Si-0.01569Si^2+0.697B+0.678P+0.473Nb+0.436S+0.168V+0.113Al+0.060Mn
+0.057Cu+0.053Mo+0.038Ni-0.047Cr (10b)

$$N(fcc + G) = \left[0.0341 - 0.0147C + 0.00171C^2\right]\cdot\sqrt{p} \quad (11)$$

$$N(Ti(C,N) + G) = 0.0308 + (Ti - 0.015)(-40.0Ti + 1.07) + (p-1)\left(-1.71\cdot10^{-3}p + 1.73\cdot10^{-2}\right) +$$
$$\left[-0.0114 + (Ti - 0.015)(17.72Ti - 0.460) + (p-1)\left(7.18\cdot10^{-4}p - 6.79\cdot10^{-3}\right)\right]\cdot C +$$
$$+\left[0.00122 + (Ti - 0.015)(-2.06Ti + 0.0559) + (p-1)\left(-8.80\cdot10^{-5}p + 7.81\cdot10^{-4}\right)\right]\cdot C^2 \quad \text{p in bar} \quad (12)$$

$$0.62 + (Ti - 0.015)(7540Ti - 231) + (p-1)(-6.32\cdot10^{-2}p + 0.488) < C <$$
$$4.2 + (Ti - 0.015)(-1684Ti + 43.0) + (p-1)(9.72\cdot10^{-3}p - 6.84\cdot10^{-2}) \quad \text{for precip. of Ti(C,N), p in bar} \quad (13a)$$

N(fcc+G) < N(Ti(C,N)+G) for precipitation of Ti(C,N) (13b)

$$NP(gas) = \left[N - \{N(fcc + G) \text{ or } N(Ti(C,N) + G)\}\right]\cdot 0.035 \quad (14)$$

$$f_G = \frac{\frac{R\cdot(T+273)}{p}\cdot NP(gas)}{\frac{R\cdot(T+273)}{p}\cdot NP(gas) + \frac{M_{Fe}}{\rho_{Fe}}\cdot NP(Liq)} \quad \text{p in atm, R = 0.0821 dm}^3\cdot\text{atm}\cdot\text{K}^{-1}\cdot\text{mol}^{-1} \quad (15)$$

$$f_{mass}(Ti(C,N), fcc) = 0.0130Ti - 3.18\cdot10^{-5} \quad (16)$$

$$f_{mass}(Ti(C,N), eutectic) = 0.0130Ti - 1.96\cdot10^{-5} \quad (17)$$